Breaking the Performance Trade-offs in Ammonia Synthesis via Spontaneous Proton Supply

Qian Wu,[a,b‡] Songzhu Luo,[b,c‡] Pengfei Song,[b] Chencheng Dai,[b,d] Leonhard Tannesia,[b,e] Longcheng Zhang,[b] Kamal Elouarzaki,[b,e] Shibo Xi,[f] Zhichuan J. Xu[b,d,e*]

[a] State Key Laboratory of Chemical Engineering, East China University of Science and Technology, Shanghai 200237, China

[b] School of Material Science and Engineering, Nanyang Technological University, 50 Nanyang Avenue, Singapore 639798, Singapore

[c] Centre of High Field NMR Spectroscopy and Imaging, Nanyang Technological University, 21 Nanyang Link, Singapore 637371, Singapore

[d] The Cambridge Centre for Advanced Research and Education in Singapore, 1 CREATE way, Singapore 138602, Singapore

[e] Center for Advanced Catalysis Science and Technology, Nanyang Technological University, 50 Nanyang Avenue, Singapore 639798, Singapore

[f] Institute of Sustainability for Chemicals, Energy and Environment (ISCE2), Agency for Science, Technology and Research (A*STAR), Singapore 627833, Singapore

*E-mail: xuzc@ntu.edu.sg

‡ These authors contributed equally to this work.

Methods

Density functional theory (DFT) calculations

Spin-polarized DFT calculations are performed with the Vienna ab initio simulation package (VASP) to evaluate Gibbs free energies.[1] Ion-electron interactions are treated with the projector-augmented plane-wave[2] and exchange-correlation interactions are described by the Perdew-Burke-Ernzerhof functional within the generalized gradient approximation.[3] Following previous reports, we consider $CoFe_{0.25}Cr_{1.75}O_4$ (110) surface with four transition mental atomic layers (bottom two layers fixed) as the calculated model, and $Co_{0.8}Fe_{0.2}(OH)_2$ (001) and (100) surfaces with four and two transition mental atomic layers (bottom two and one layers fixed, respectively) as the calculated model, respectively.[4] The slabs are separated by a vacuum space of at least 15 Å along the z axis and a (3 × 3 × 1) Monkhorst−Pack k-point grids are used. Grimme's D3 method is adopted to account for van der Waals (vdW) interactions.[5] The cut-off energy is set as 550 eV, and all systems are optimized until energy and force are less than 10^{-5} eV and 0.01 eV/Å. The computational results are carried out with VASPKIT.[6]

The Gibbs free energy of each elemental step (ΔG) of the NO_3RR is adopted following the works of Nørskov et al.[7,8]

$$\Delta G = \Delta E + \Delta E_{ZPE} - T\Delta S - eU + 0.059\times pH$$

where ΔE is the changed energy, ΔE_{ZPE} and ΔS are the change of zero-point vibrational energy and the change of entropy, respectively, which can be obtained by the vibrational frequency of the optimized structures. T is the temperature and set to 298.15 K, e and U are the transferred charge and the electrode potential, respectively. The pH is set as 14 in accordance with the experimental environments.

Constant Potential Method. Constant potential method is employed to simulate the applied potential effect on the NO_3RR potential-determining step on A-$CoFe_{0.25}Cr_{1.75}O_4$.[9] The aqueous environment is modeled as a continuum dielectric by the VASPsol code.[10] Charges ranging from −1.5 e to +1.5 e is added in steps of 0.5 e for each system to clarify the applied potential function. The potential-dependent energy can be calculated as[11]

$$U_q = -4.6 - \varphi_q/eV$$

where 4.6 V is the absolute potential relative to the SHE benchmarked in the VASPsol.[12]

The energy varies with the electrode potential as a quadratic function,

$$E(U_q) = -\frac{1}{2}C(U_q - U_0)^2 + E_0$$

where C is the capacitance of the system, U_0 is the potential of zero charges (PZC), and E_0 is the energy at the zero charges.

Material synthesis

$CoFe_{0.25}Cr_{1.75}O_4$ spinel oxide powders are synthesized by traditional sol-gel methods. Taking the preparation of 10 mmol $CoFe_{0.25}Cr_{1.75}O_4$ as an example, 10 mmol $Co(NO_3)_2 \cdot 6H_2O$ (Nickel(II) nitrate hexahydrate, crystals or chunks, Sigma Aldrich), 2.5 mmol $Fe(NO_3)_3 \cdot 9H_2O$ (Iron(III) nitrate nonahydrate, ACS reagent, ≥98%, Sigma-Aldrich) and 17.5 mmol $Cr(NO_3)_3 \cdot 9H_2O$ (Chromium(III) nitrate nonahydrate, 99%, Sigma-Aldrich) are dissolved using minimum deionized water (DI water) with magnetic stirring in a 1-liter glassy beaker. Then, both 30 mmol EDTA (Ethylenediaminetetraacetic acid, BioUltra, anhydrous, ≥99% (titration), Sigma-Aldrich) and 60 mmol $C_6H_8O_7 \cdot H_2O$ (Citric acid monohydrate, ACS reagent, ≥99.0%) are added into solutions subsequently.

The pH is adjusted with NH_4OH (Ammonium hydroxide solution, Ammonium hydroxide solution, puriss., 25−30% NH_3 basis, Sigma-Aldrich) under stirring until a clear solution is obtained. The solution is heated at 200 °C until a gel is formed, followed by drying at 250 °C overnight. The dried precursor is ground to a powder and calcined in air at 1000 °C for 10 h (ramp rate of 5 °C min^{-1}). After furnace cooling, the product is ground to yield the final powder.

Materials characterization

Phase identification of $CoFe_{0.25}Cr_{1.75}O_4$ is performed using X-ray powder diffraction (Bruker D8 Advance, Cu Kα, λ = 1.5418 Å) with a scan rate of 2° min^{-1}. High-resolution transmission electron microscopy (HRTEM) images are acquired on a JEOL JEM-2100F operated at 200 kV. X-ray photoelectron spectroscopy (XPS) measurements are conducted on a PHI-5400 system using an Al Kα source (250 W) with a position-sensitive detector. Co K-edge X-ray absorption near-edge structure (XANES) and extended X-ray absorption fine structure (EXAFS) spectra are collected in transmission mode at the X-ray Absorption Fine-structure for Catalysis (XAFCA) beamline of the Singapore Synchrotron Light Source. Data reduction and analysis are performed with the Athena package.

Electrochemical measurement

Electrocatalyst pre-activation is conducted in a single-cell setup; all other electrochemical tests use a custom H-cell separated by a Nafion 117 membrane (DuPont) at ambient conditions. Before using the membrane, it is soaked in 5 wt% H_2O_2 solution at 80 °C for 1 hour first, then it is soaked in 5 wt% H_2SO_4 solution at 80 °C for 1 hour, later it is soaked in deionized water for an hour at 80 °C. A Biologic-SP150 potentiostat is used to record the electrochemical response. In the typical three-electrode system, a glassy carbon electrode (the glassy carbon electrode is a disk electrode with a diameter of Φ=5 mm. The exposed geometric electrode area is calculated from the disk area, $A=\pi d^2/4$, giving an area of 0.196 cm^2), a Hg/HgO electrode and a platinum plate electrode are used as the working electrode, reference and counter electrode, respectively. The Hg/HgO reference is calibrated in 1 M KOH following literature procedures. Solution resistance is determined by potentiostatic electrochemical impedance spectroscopy (200 kHz to 0.1 Hz).

Catalyst inks are prepared by dispersing 25 mg catalyst, 12.5 mg acetylene black, 3.875 mL deionized water, 1.0 mL isopropyl alcohol, and 125 µL Nafion solution (5 wt%) by sonication for ≥ 2 h. An 8 µL aliquot is drop-cast onto the glassy carbon electrode, yielding a loading of 204.1 µg cm^{-2}. Pre-activation of $CoFe_{0.25}Cr_{1.75}O_4$ is performed by chronoamperometry at 1.6 V vs. RHE for 2 h in 1 M KOH. For nitrate reduction (NO_3RR), 40 mL of 1 M KOH + 0.1 M KNO_3 is used in each H-cell compartment. The electrolyte is purged with Ar for 30 min prior to testing. Cyclic voltammetry (CV) is recorded at 10 mV s^{-1}. The NO_3RR is measured at a stirring rate of 600 rpm in the cathodic chamber. FE and NH_3 yield rate are evaluated at potentials from −0.2 to −0.6 V vs. RHE in 0.1 V increments using 30-min potentiostatic holds. Potentials are converted to the RHE scale according to E (V vs. RHE) = E (vs. Hg/HgO) + 0.098 + 0.0591 × pH (25 °C), unless otherwise specified. All electrochemical measurements are repeated independently three times. The data are reported as mean ± standard deviation, and the error bars represent the standard deviation derived from three independent measurements.

Product analysis

Ammonia detection NH_3 concentrations are determined by the indophenol blue method. Electrolyte samples are withdrawn and diluted to the calibration range. A 2 mL aliquot of the diluted solution is mixed with 2 mL of 1 M KOH containing 5 wt% salicylic acid and 5 wt% potassium citrates. Next, 1 mL of 0.05 M KClO and 0.2 mL of 1.0 wt% $C_5FeN_6K_2O$ (potassium nitroferricyanide) solution are added. After 2 h at room temperature, absorbance at 655 nm was measured on a UV-2600 spectrophotometer and converted to NH_3 concentration using a calibration curve.[13]

Nitrite detection A color reagent is prepared by dissolving 0.2 g N-(1-naphthyl)ethylenediamine dihydrochloride, 4 g p-aminobenzenesulfonamide, and 10 mL phosphoric acid (ρ = 1.685 g mL^{-1}) in 50 mL deionized water with thorough stirring. Electrolyte samples are diluted to the calibration range, and 5 mL of the diluted sample is combined with 0.1 mL color reagent. After 20 min at room temperature, the absorbance at 540 nm is recorded.[13] Nitrite concentrations are obtained from calibration with standard KNO_2 solutions.

FE and yield rate

Faradaic efficiency (FE) is calculated as:

$$FE = \frac{ncV_{catholyte}F}{Q} \times 100\%$$

where n is the electron-transfer number (8 for NH_3, 2 for NO_2^-), c is the concentration of NH_3 or NO_2^-, $V_{catholyte}$ is the catholyte volume (40 mL), F is the Faradaic constant (96485 C mol^{-1}), and Q is the total charge passed.

Yield rate is calculated as:

$$Yield = \frac{cV_{catholyte}}{St}$$

where S is the geometric area of the cathode, and t is the electrolysis time (30 min).

Electrochemical in-situ ATR-FTIR

In situ ATR-FTIR spectra are acquired following our previous procedure[14] using a Bruker Vertex 80 coupled to a PIKE VeeMAX III electrochemical accessory. A liquid-nitrogen-cooled mercury cadmium telluride (MCT) detector is employed. The internal reflection element is a Si prism coated by e-beam evaporation with Ti (5 nm) and Au (25 nm), used at an incidence angle of 60°. Catalysts are drop-cast on the prism to a loading of 0.2 mg cm^{-2} and served as the working electrode. An Ag/AgCl (sat. KCl) reference and a graphite rod counter electrode are used. The electrolyte is 1 M KOH + 0.1 M KNO_3. Spectra are collected during chronoamperometry at the indicated potentials.

Electrochemical impedance spectroscopy

Electrochemical impedance spectroscopy is performed to evaluate the interfacial charge-transfer behavior of $CoFe_{0.25}Cr_{1.75}O_4$, A-$CoFe_{0.25}Cr_{1.75}O_4$, and $Co_{0.8}Fe_{0.2}(OH)_2$ during nitrate reduction. The Nyquist plots are fitted using a modified Randles circuit, $R_s - (R_{ct} \parallel CPE_{dl})$, where R_s represents the solution resistance, R_{ct} denotes the charge-transfer resistance associated with the faradaic NO_3^- reduction process, and CPE_{dl} describes the non-ideal double-layer capacitance at the electrode/electrolyte interface, n is the CPE exponent. The fitted R_s values are similar for the three samples, ranging from 5.02 to 5.60 Ω, indicating comparable ohmic resistance under the same electrolyte and cell configuration. In contrast, the R_{ct} value decreases markedly from 61.79 Ω for $CoFe_{0.25}Cr_{1.75}O_4$ to 10.21 Ω for A-$CoFe_{0.25}Cr_{1.75}O_4$ and 9.43 Ω for $Co_{0.8}Fe_{0.2}(OH)_2$, revealing substantially improved interfacial charge-transfer kinetics after activation/reconstruction and for the $Co_{0.8}Fe_{0.2}(OH)_2$ reference. The much smaller $R_{ct}$of A-$CoFe_{0.25}Cr_{1.75}O_4$ compared with $CoFe_{0.25}Cr_{1.75}O_4$ suggests that the activated surface provides a more favorable interface for electron transfer during NO_3RR. In addition, the use of CPE_{dl} rather than an ideal capacitor accounts for the depressed semicircular response, which is commonly associated with surface heterogeneity, roughness, distributed active sites, and non-uniform adsorption environments on electrocatalyst surfaces. Therefore, the EIS results support that activation/reconstruction effectively lowers the

interfacial kinetic barrier and facilitates NO_3RR.

Turnover frequency calculations

The TOF is calculated according to the equation: $T = j*A*FE_{NH3}/(8*F*n)$, Where j is the current density normalized by BET surface area, A is the BET surface area; F is the Faraday constant (96485 C mol^{-1}); n is the mole number of active atoms on the electrode. The number of active sites (n) is calculated as: $n_{bulk} = m_{ox}/M_{ox}$, where m_{ox} is the mass of the catalyst, M_{ox} is the molecular weight of the catalyst. Take $CoFe_{0.25}Cr_{1.75}O_4$ as an example, to convert n_{bulk} to n, if Co+Fe is assumed to be the active sites, $n = 1.25 \times n_{bulk}$.

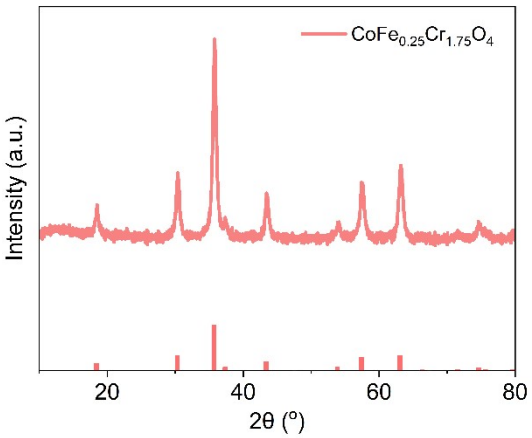

Fig. S1 XRD pattern of $CoFe_{0.25}Cr_{1.75}O_4$.

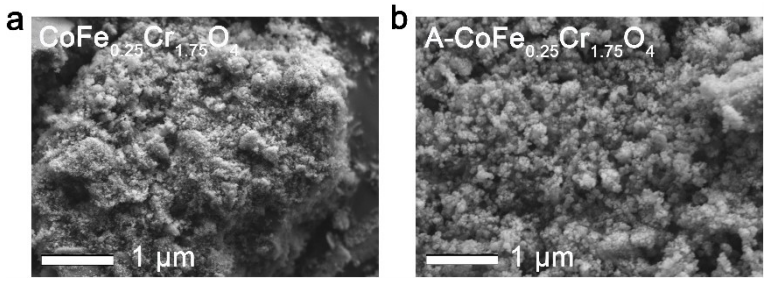

Fig. S2 SEM images of **a** $CoFe_{0.25}Cr_{1.75}O_4$, and **b** activated $CoFe_{0.25}Cr_{1.75}O_4$ (A-$CoFe_{0.25}Cr_{1.75}O_4$).

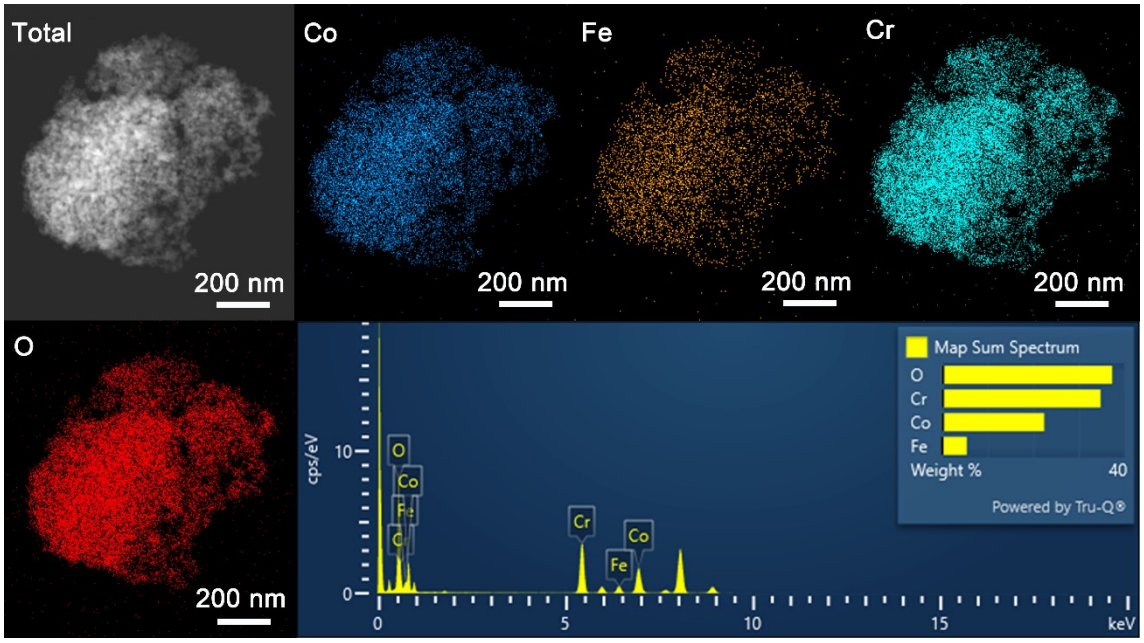

Fig. S3 EDS mapping images of $CoFe_{0.25}Cr_{1.75}O_4$.

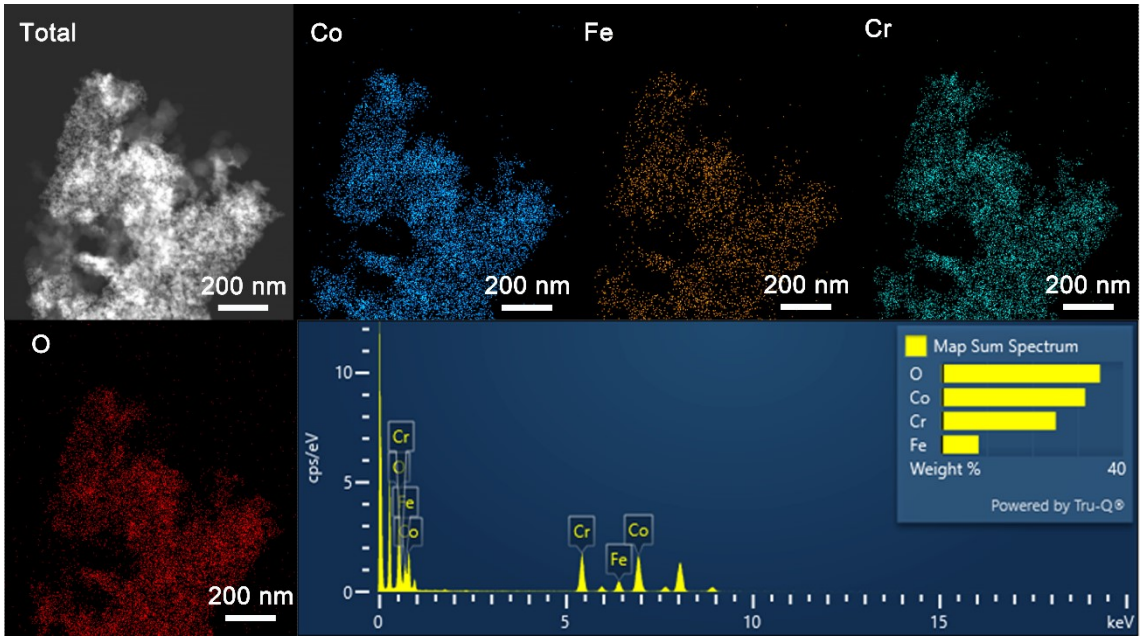

Fig. S4 EDS mapping images of A-$CoFe_{0.25}Cr_{1.75}O_4$.

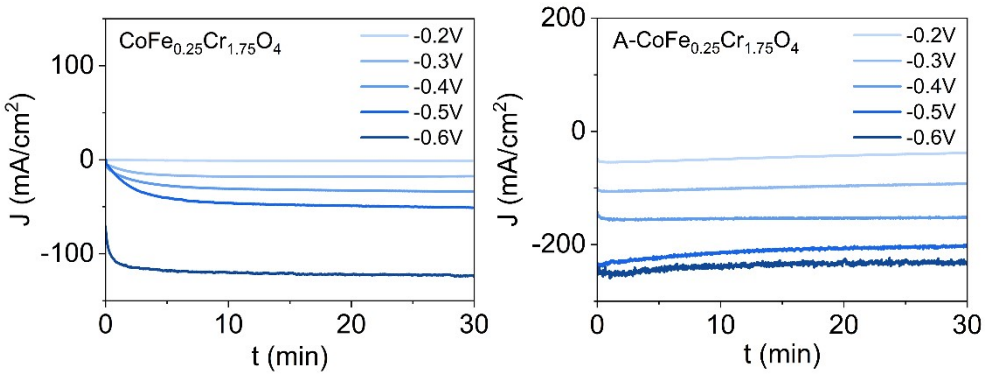

Fig. S5 Chronoamperometry curves of $CoFe_{0.25}Cr_{1.75}O_4$ and A-$CoFe_{0.25}Cr_{1.75}O_4$ in 1 M KOH + 0.1 M KNO_3 electrolyte under different potentials in H-cell.

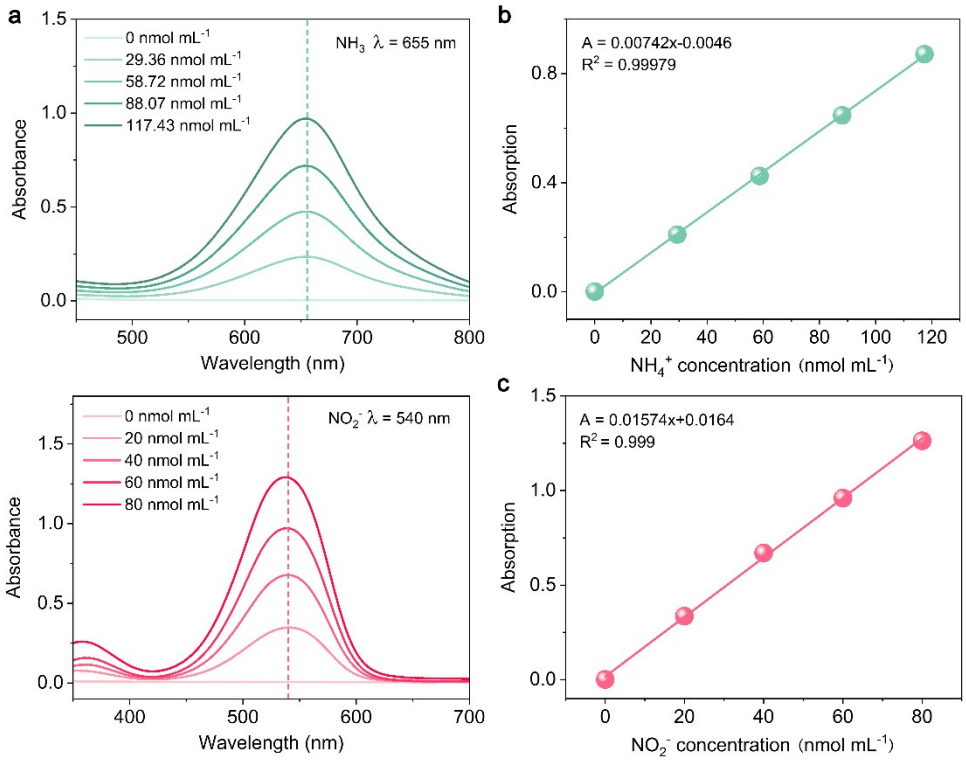

Fig. S6 UV-vis curves of **a** NH_4^+ and **c** NO_2^-. **b** Calibration curve at 655 nm for different NH_4^+ concentrations. **d** Calibration curve at 540 nm for different NO_2^- concentrations.

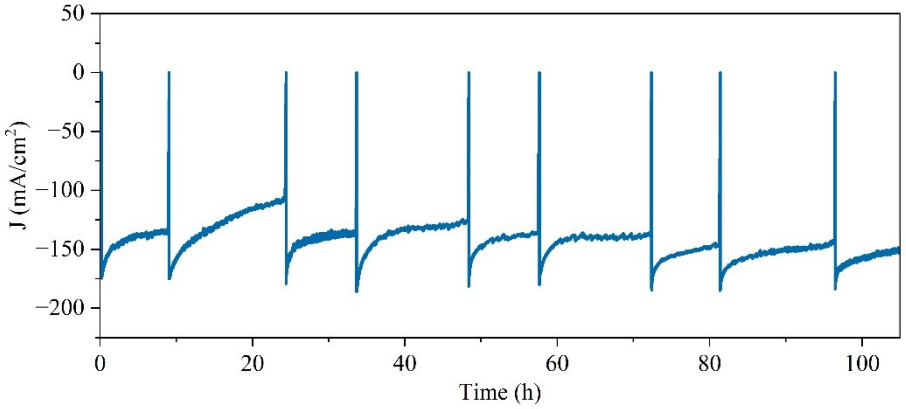

Fig. S7 Long-term CA stability test (larger 100 hours) for A-$CoFe_{0.25}Cr_{1.75}O_4$ at −0.4 V/RHE. The periodic spikes in the current curve indicate electrolyte repositioning.

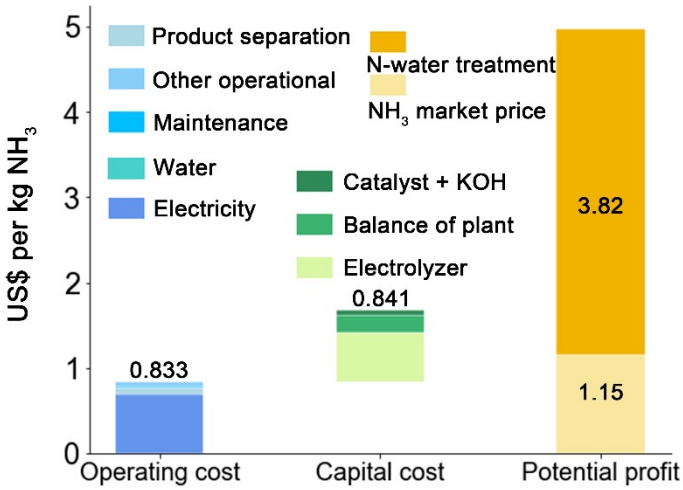

Fig. S8 Breakdown of production cost of NH_3 synthesis by NO_3RR and its potential profits. The total cost is US$1.674 per kg NH_3. Potential profits include selling NH_3 at the market price as well as the operational expenses of wastewater treatment through nitrate removal.

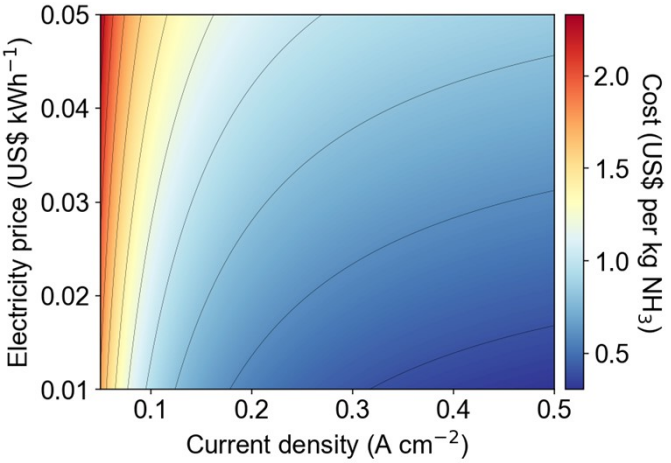

Fig. S9 Contour map for NH_3 synthesis costs as a function of current density and electricity price.

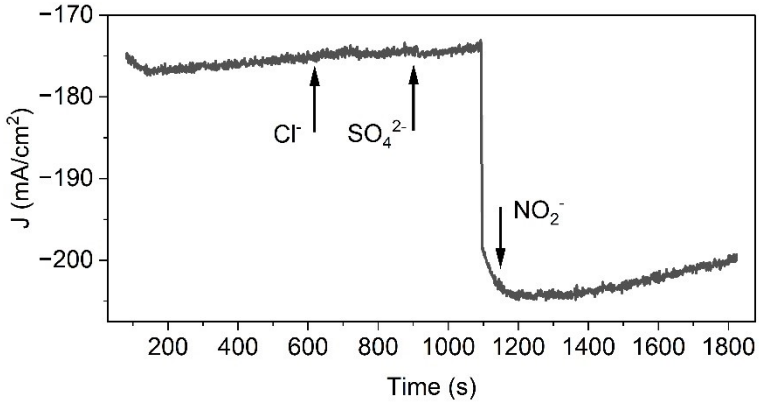

Fig. S10 Stability test using interfering ions (Cl^{-}, SO_4^{2-} and NO_2^{-}).

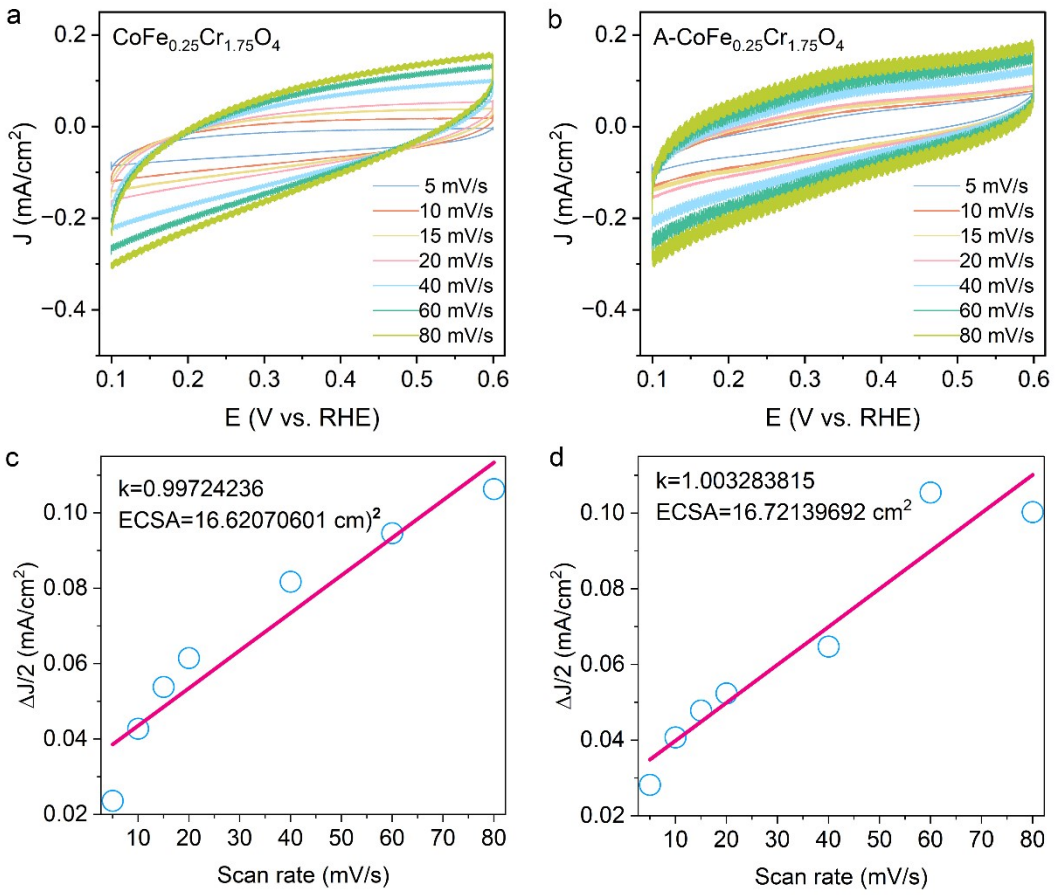

Fig. S11 CV curves of (a) $CoFe_{0.25}Cr_{1.75}O_4$, (b) A-$CoFe_{0.25}Cr_{1.75}O_4$, and the corresponding fitting of (c) $CoFe_{0.25}Cr_{1.75}O_4$ and (d) A-$CoFe_{0.25}Cr_{1.75}O_4$ to obtain double-layer capacitances at scan rates of 80, 60, 60, 40, 20, 15 10 and 5mV s^{-1} in 1 M KOH. The geometry area of the working electrode (glassy carbon) is 0.196 cm^2, and the catalyst loading is 0.2 mg cm^{-2}.

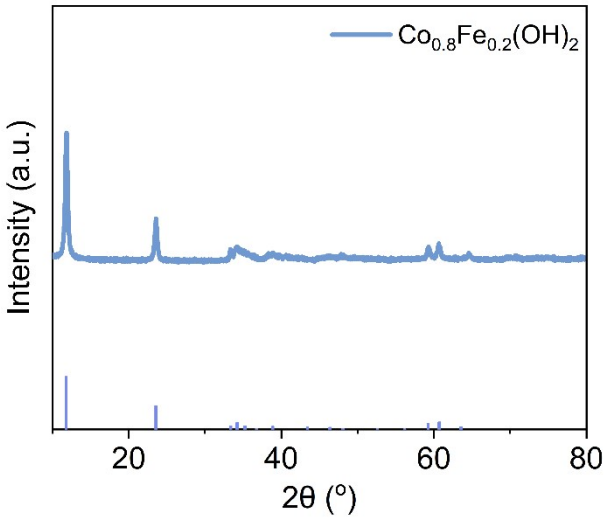

Fig. S12 XRD pattern of $Co_{0.8}Fe_{0.2}(OH)_2$.

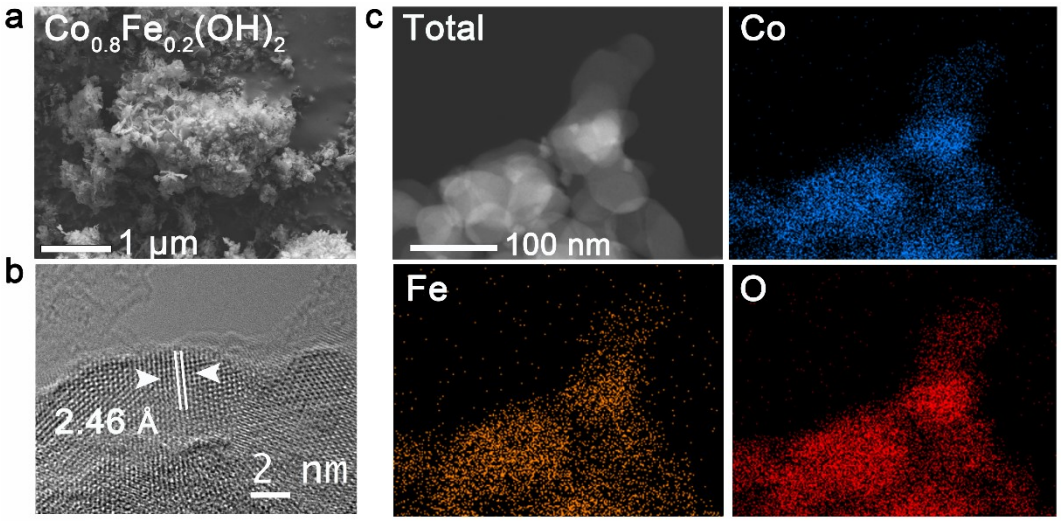

Fig. S13 a SEM, **b** HRTEM, and corresponding **c** EDS mapping images of $Co_{0.8}Fe_{0.2}(OH)_2$.

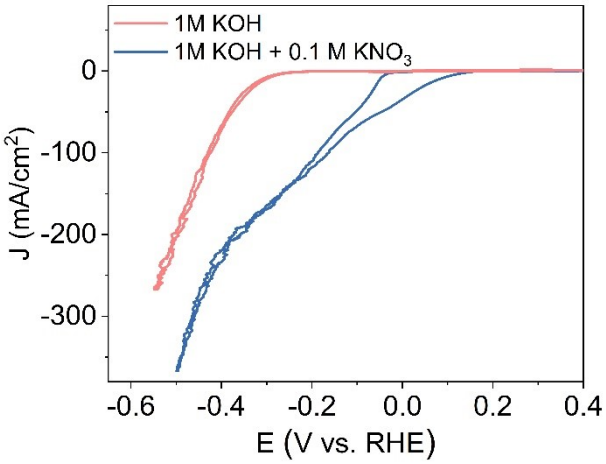

Fig. S14 Cyclic voltammetry curves of $Co_{0.8}Fe_{0.2}(OH)_2$.

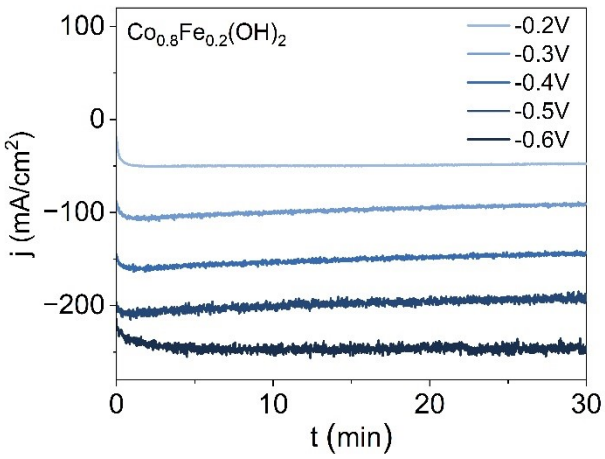

Fig. S15 Chronoamperometry curves of $Co_{0.8}Fe_{0.2}(OH)_2$ in 1 M KOH + 0.1 M KNO_3 electrolyte under different potentials in H-cell.

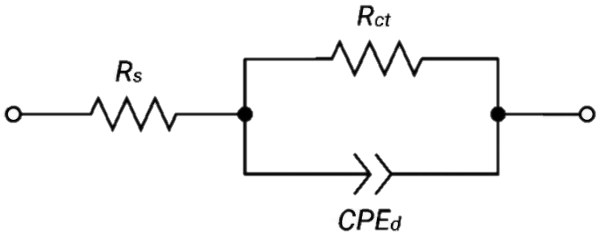

Fig. S16 Equivalent circuit for electrochemical impedance spectroscopy.

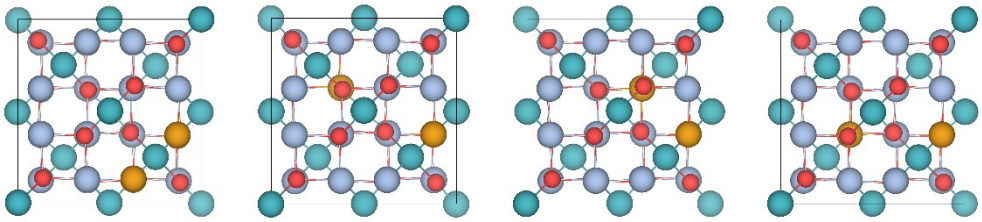

Fig. S17 Possible structure configurations of bulk $CoFe_{0.25}Cr_{1.75}O_4$. Red, orange, light bule and blue atoms indicate the oxygen, iron, chromium, and cobalt atoms.

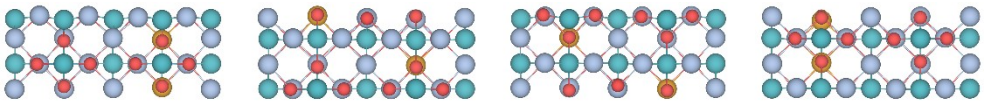

Fig. S18 Possible configurations of $CoFe_{0.25}Cr_{1.75}O_4$ (1 1 0) surface. Red, orange, light blue and blue atoms indicate the oxygen, iron, chromium, and cobalt atoms.

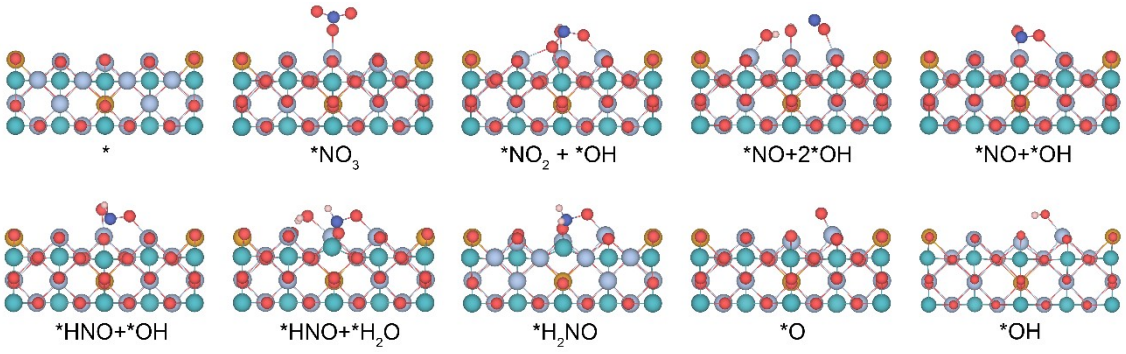

Fig. S19 The most stable configurations of intermediates on $CoFe_{0.25}Cr_{1.75}O_4$ (110) surface during NO_3RR. Red, orange, light bule, blue, dark blue, and pink atoms indicate the oxygen, iron, chromium, cobalt, nitrogen and hydrogen atoms.

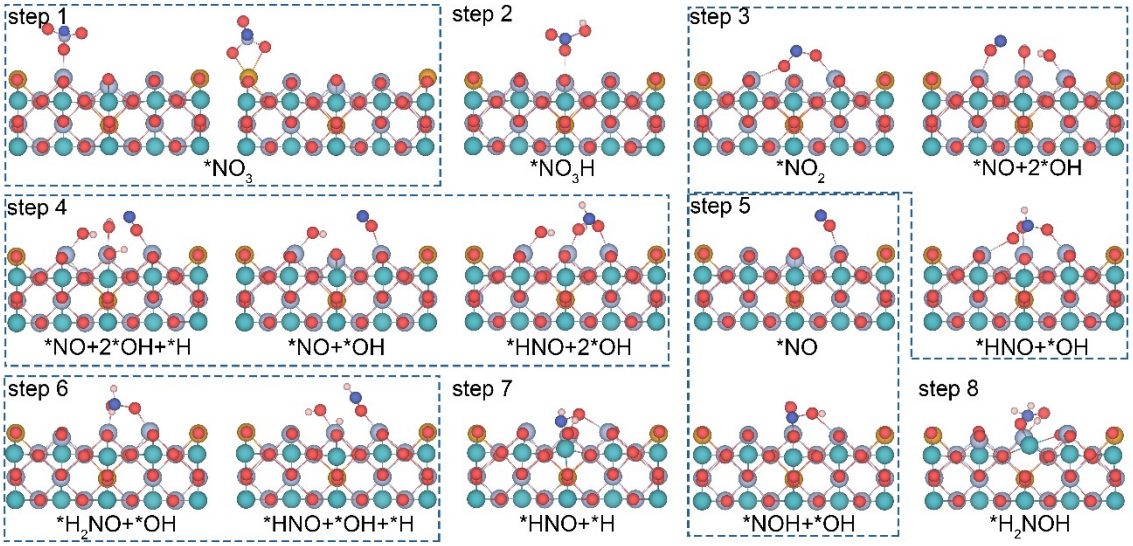

Fig. S20 The other possible configurations of intermediates on $CoFe_{0.25}Cr_{1.75}O_4$ (110) surface during NO_3RR. Red, orange, light blue, blue, dark blue, and pink atoms indicate the oxygen, iron, chromium, cobalt, nitrogen and hydrogen atoms.

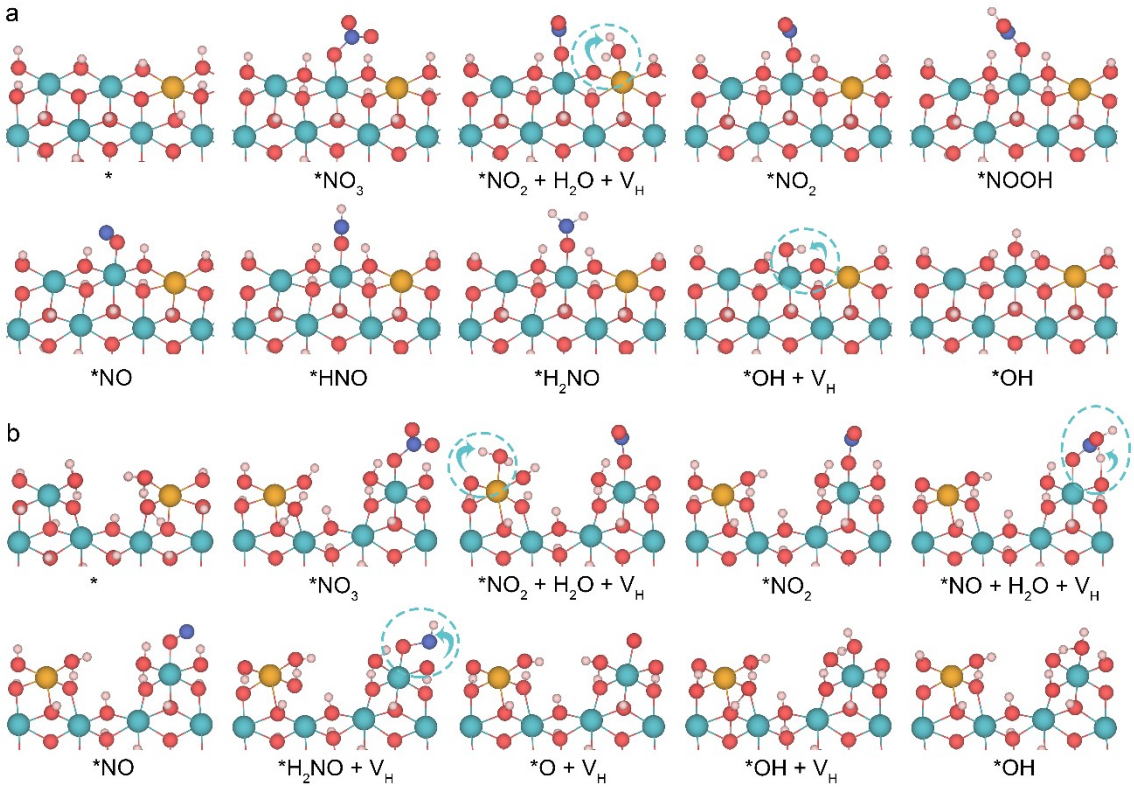

Fig. S21 The most stable configurations of intermediates on **a** $Co_{0.8}Fe_{0.2}(OH)_2$ and **b** A-$CoFe_{0.25}Cr_{1.75}O_4$ (100) surfaces during NO_3RR. Red, orange, blue, dark blue, and pink atoms indicate the oxygen, iron, cobalt, nitrogen and hydrogen atoms.

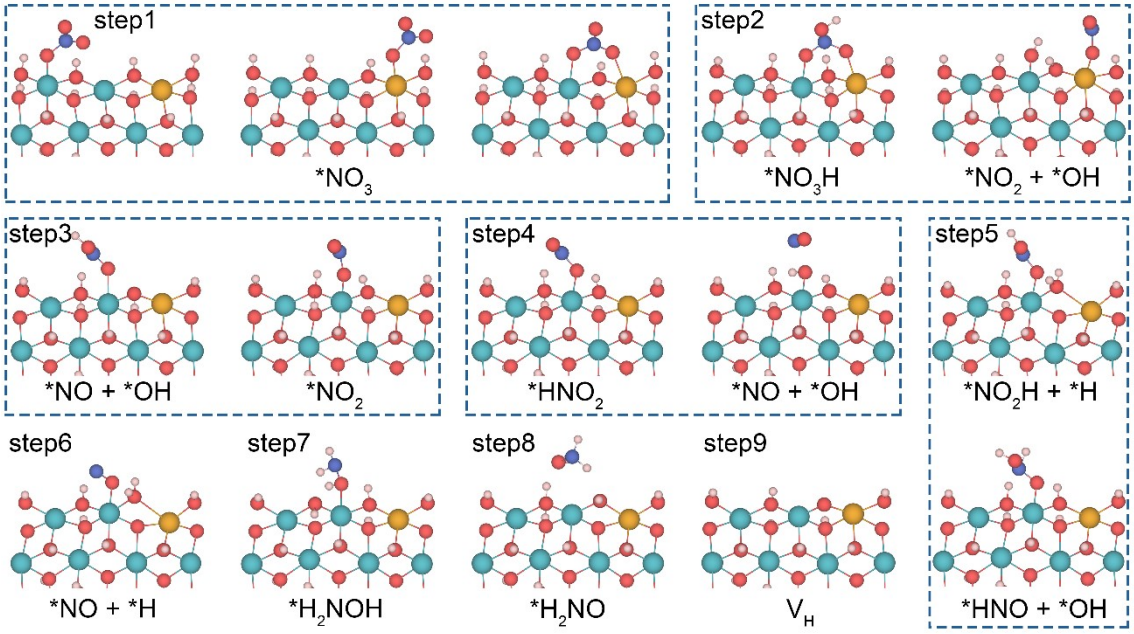

Fig. S22 The other possible configurations of intermediates on $Co_{0.8}Fe_{0.2}(OH)_2$ (100) surface during NO_3RR. Red, orange, blue, dark blue, and pink atoms indicate the oxygen, iron, cobalt, nitrogen and hydrogen atoms.

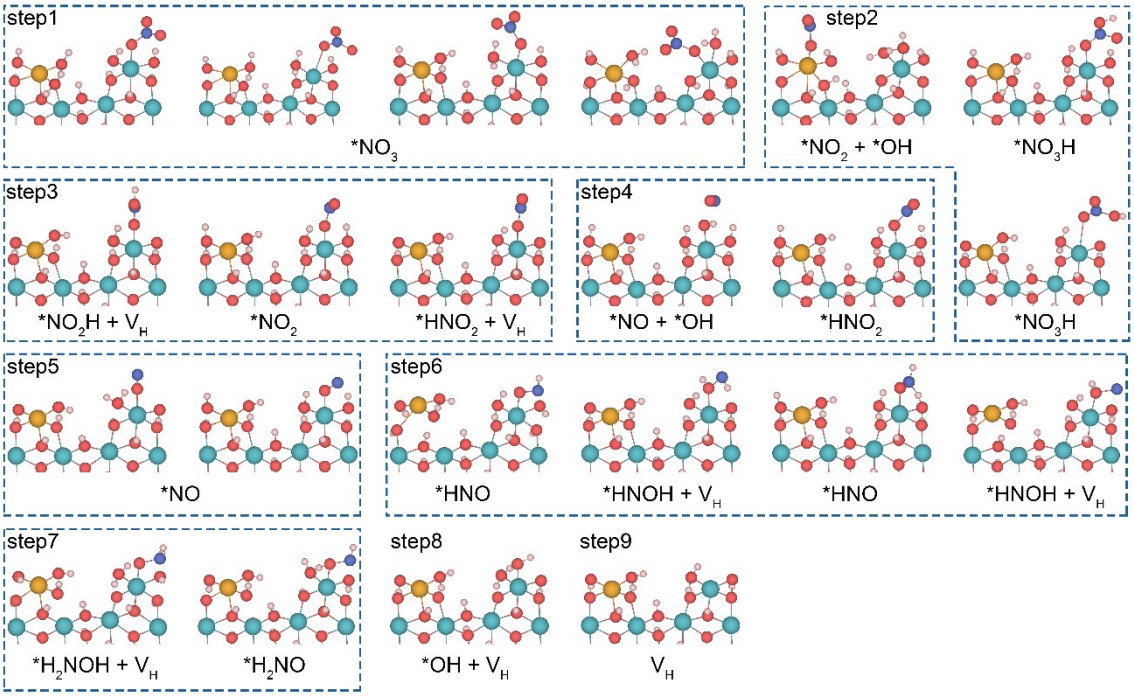

Fig. S23 The possible configurations of intermediates on A-$CoFe_{0.25}Cr_{1.75}O_4$ (100) surface during NO_3RR. Red, orange, blue, dark blue, and pink atoms indicate the oxygen, iron, cobalt, nitrogen and hydrogen atoms.

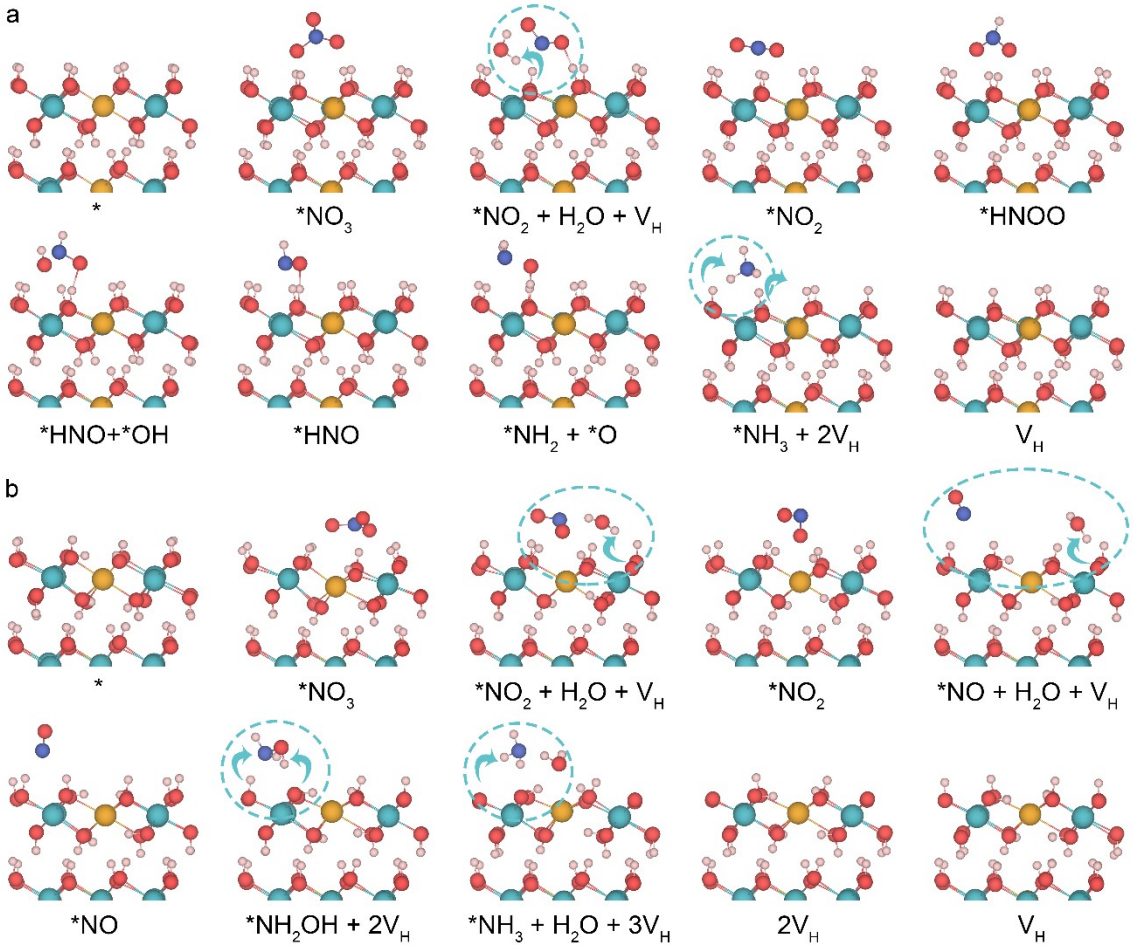

Fig. S24 The most stable configurations of intermediates on **a** $Co_{0.8}Fe_{0.2}(OH)_2$ and **b** A-$CoFe_{0.25}Cr_{1.75}O_4$ (001) surfaces during NO_3RR. Red, orange, blue, dark blue, and pink atoms indicate the oxygen, iron, cobalt, nitrogen and hydrogen atoms.

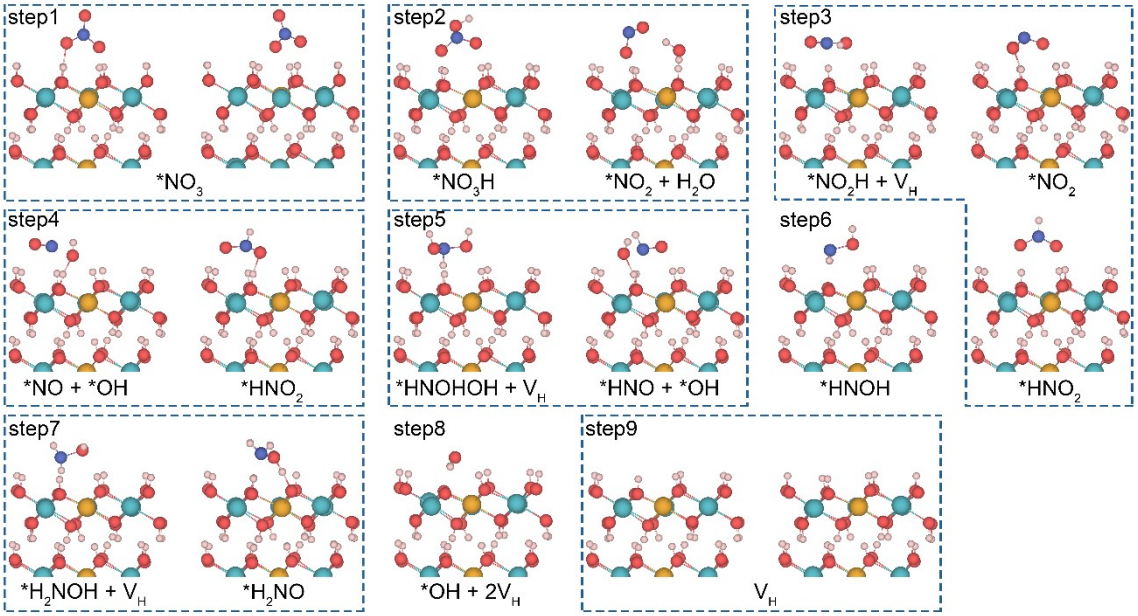

Fig. S25 The other possible configurations of intermediates on $Co_{0.8}Fe_{0.2}(OH)_2$ (001) surface during NO_3RR. Red, orange, blue, dark blue, and pink atoms indicate the oxygen, iron, cobalt, nitrogen and hydrogen atoms.

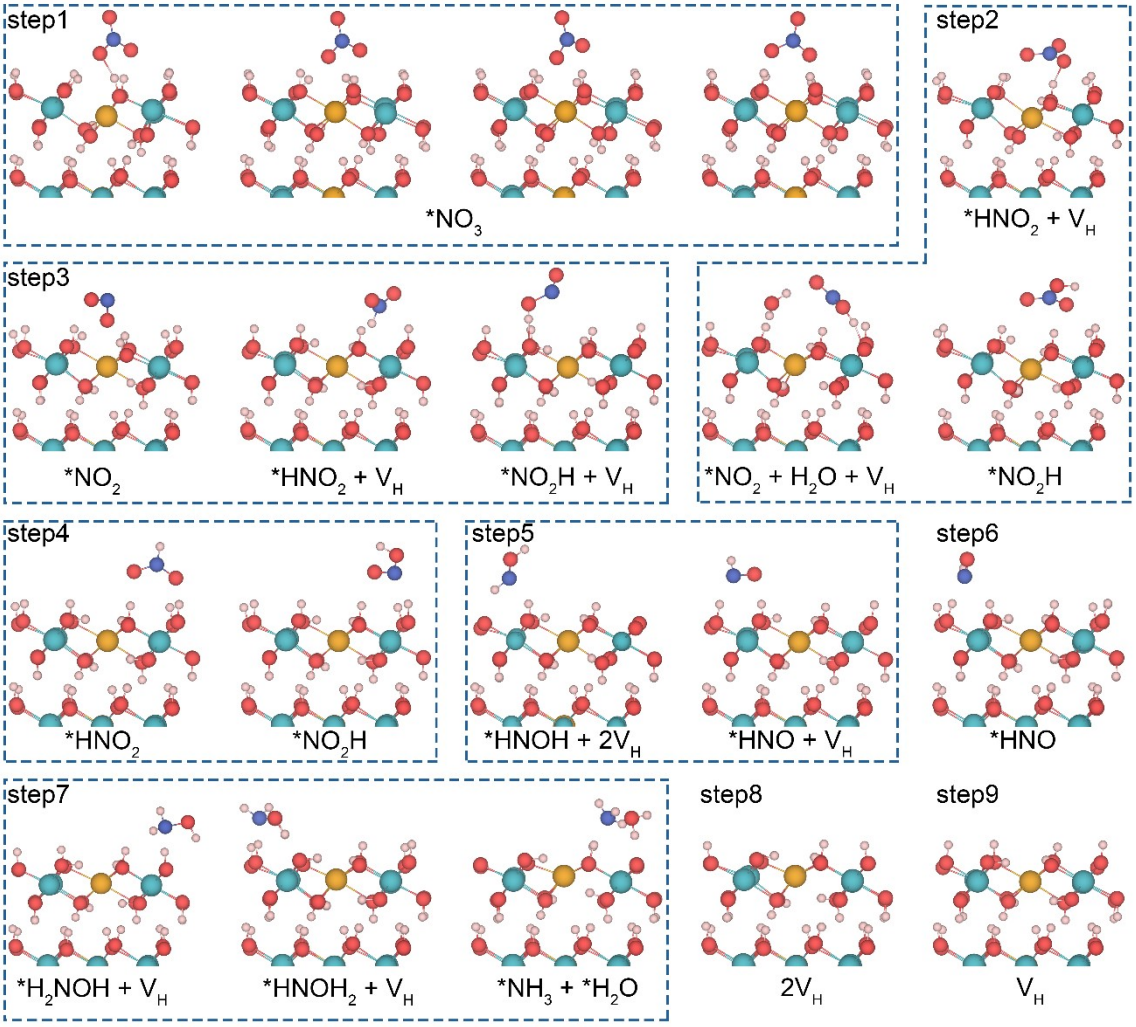

Fig. S26 The other possible configurations of intermediates on A-$CoFe_{0.25}Cr_{1.75}O_4$ (001) surface during NO_3RR. Red, orange, blue, dark blue, and pink atoms indicate the oxygen, iron, cobalt, nitrogen and hydrogen atoms.

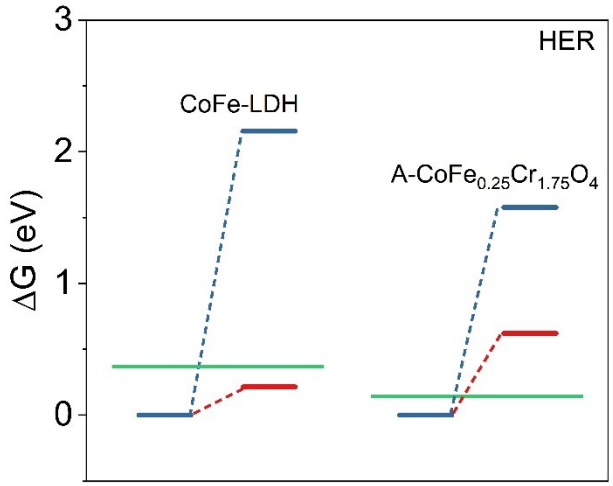

Fig. S27 Gibbs free energies of the hydrogen evolution reaction on $Co_{0.8}Fe_{0.2}(OH)_2$ and A-$CoFe_{0.25}Cr_{1.75}O_4$. Blue and red lines indicate whether the protons in the generated H_2 are single proton or two protons from lattice-hydrogen. Green line indicates the limiting potential of NO_3RR on $Co_{0.8}Fe_{0.2}(OH)_2$ and A-$CoFe_{0.25}Cr_{1.75}O_4$.

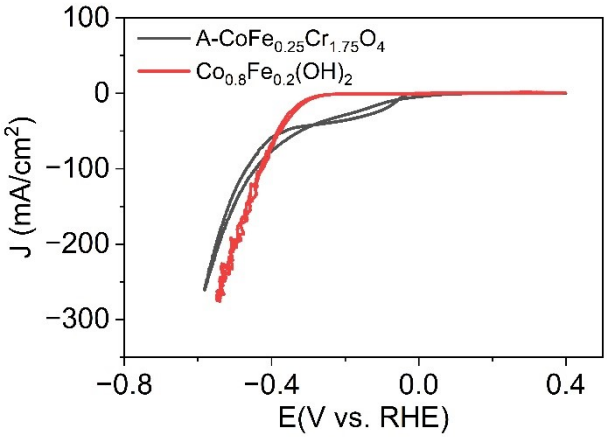

Fig. S28 Cyclic voltammetry curves of A-$CoFe_{0.25}Cr_{1.75}O_4$ and $Co_{0.8}Fe_{0.2}(OH)_2$ in 1 M KOH electrolyte.

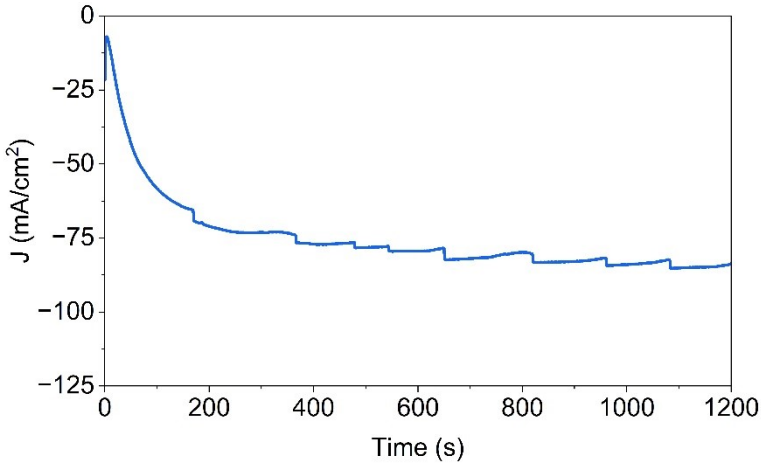

Fig. S29 Chronoamperometry curves for A-$CoFe_{0.25}Cr_{1.75}O_4$ at −0.2 V/RHE in 1 M KOH electrolyte.

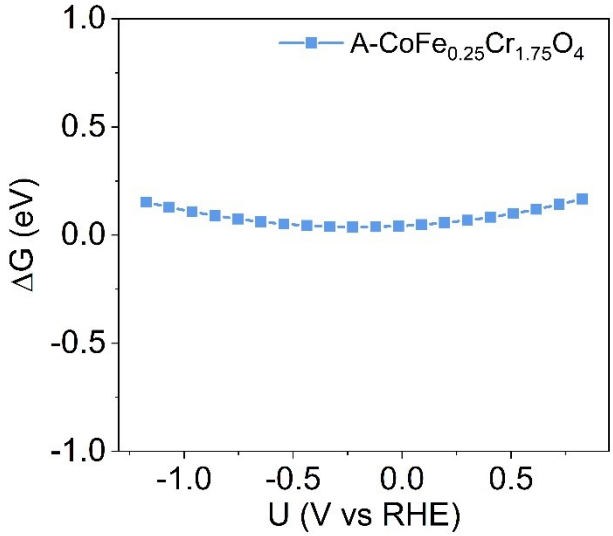

Fig. S30 The constant potential calculation of NO_3RR potential-determining step on A-$CoFe_{0.25}Cr_{1.75}O_4$.

Table S1. Curve fit parameters[a] for Co *K*-edge EXAFS of pristine $CoFe_{0.25}Cr_{1.75}O_4$.

Path	*d* [b]/Å	*N*	*R*/ Å	σ^2/Å^2
Co-O	1.943	4.4(2)	1.97(2)	0.003(3)

[a]S_0^2 is fixed as 0.74703, obtained from Co foil fitting. ΔE_0 is refined as a global fit parameter, returning a value of (4 ± 1) eV. Data ranges: $3 \leq k \leq 12$ Å^{-1}, $1.0 \leq R \leq 2.0$ Å. The number of variable parameters is 4, out of a total of 5.59 independent data points. R factor for this fit is 0.16%. [b]The distance is from the crystal structure of Co_2O_3. [c]The Debye-Waller factor was fixed to reduce the number of variables.

Table S2. Curve fit parameters[a] for Co *K*-edge EXAFS of A-$CoFe_{0.25}Cr_{1.75}O_4$.

Path	*d* [b]/Å	*N*	*R*/ Å	σ^2/Å^2
Co-O	1.943	4.5(2)	1.95(6)	0.003[c]

[a]S_0^2 is fixed as 0.74703, obtained from Co foil fitting. ΔE_0 is refined as a global fit parameter, returning a value of (3 ± 1) eV. Data ranges: $3 \leq k \leq 12$ Å^{-1}, $1.0 \leq R \leq 2.0$ Å. The number of variable parameters is 3, out of a total of 5.5 independent data points. R factor for this fit is 0.4%. [b]The distance is from the crystal structure of Co_2O_3. [c]The Debye-Waller factor is fixed to reduce the number of variables.

Table S3. Curve fit parameters[a] for Co *K*-edge EXAFS for $CoFe_{0.25}Cr_{1.75}O_4$ after reaction.

Path	*d* [b]/Å	*N*	*R*/ Å	σ^2/Å^2
Co-O	1.943	4.5(3)	1.97(9)	0.004[c]

[a]S_0^2 is fixed as 0.74703, obtained from Co foil fitting. ΔE_0 is refined as a global fit parameter, returning a value of (4 ± 1) eV. Data ranges: $3 \leq k \leq 12$ Å^{-1}, $1.0 \leq R \leq 2.0$ Å. The number of variable parameters is 3, out of a total of 5.5 independent data points. R factor for this fit is 1.2%. [b]The distance is from the crystal structure of Co_2O_3. [c]The Debye-Waller factor is fixed to reduce the number of variables.

Table S4. Curve fit parameters[a] for Co *K*-edge EXAFS for pristine $Co_{0.8}Fe_{0.2}(OH)_2$.

Path	*d* [b]/Å	*N*	*R*/ Å	σ^2/Å^2
Co-O	2.097	6.0[c]	2.07(2)	0.006(2)

[a]S_0^2 is fixed as 0.74703, obtained from Co foil fitting. ΔE_0 is refined as a global fit parameter, returning a value of (3 ± 1) eV. Data ranges: $3 \leq k \leq 12$ Å^{-1}, $1.0 \leq R \leq 2.1$ Å. The number of variable parameters is 3, out of a total of 6.0 independent data points. R factor for this fit is 2.4%. [b]The distance is from the crystal structure of α-$Co_{0.8}Fe_{0.2}(OH)_2$. [c]The coordination number is fixed to reduce the number of variables.

Technoeconomic analysis (TEA)

Table S5 Input parameters for the TEA model.

NH_3 production rate	1,000 kg day^{-1}
Operating time	350 days year^{-1}
Electrolyzer base cost[15]	550 USD kW^{-1}
Balance of plant[16]	35% of the electrolyzer cost
Maintenance cost[17]	2.5% of the electrolyzer cost

Installation cost	12% of the electrolyzer cost
Catalysts cost	5% of the electrolyzer cost
KOH cost	5% of the electrolyzer cost
Product separation costs	10% of the electricity cost
Other operational costs	10% of the electrolyzer cost
Plant lifetime	20 years
Discount rate	5%
Electric price (USD kWh^{-1})[18]	0.03

Noted: The total cost is separated into 7 components, namely the **capital cost, electricity cost**, **maintenance cost**, **product separation cost**, **water cost, balance of plant cost** and **other operational costs**.[19,20]

For 0.1 M $NaNO_3$:

The charge required to produce per 1000 kg NH_3:

$$Q = \frac{n(NH_3) \times N \times F}{FE} = \frac{1 \times 10^6 g \times 8 \times 96485 \frac{C}{mol}}{17 \frac{g}{mol} \times 0.94} = 4.825 \times 10^{10} C$$

The current required to sustain the process:

$$I = \frac{Q}{t} = \frac{4.825 \times 10^{10} C}{86400 s} = 558449 A$$

Area of electrolyzer:

$$area = \frac{I}{0.096\ Acm^{-2}} = \frac{558449 A}{0.096\ Acm^{-2}} = 581.7 m^2$$

Based on the E4tech/Element Energy report[15] and DOE H2A analysis for central grid electrolysis,[16] the electrolyzer cost for the stack component is 550 USD kW^{-1} with a reference current density of 400 mA cm^{-2} at 1.75 V. The total **electrolyzer cost** is calculated as:

$$Electrolyzer\ cost = \frac{550\ USD\ kW^{-1}}{1000 \frac{W}{kW}} \times \frac{400 mA cm^{-2}}{1000 \frac{mA}{A}} \times 1.75 V \times \frac{581.7 m^2}{0.0001 \frac{m^2}{cm^2}} \times 1.12 = 2508290.4\ USD$$

Considering the capital recovery factor (CRF) based on a 5% discount rate (denote as i in the equation below), with the lifetime of 20 years:

$$CRF = \frac{i(1+i)^{20}}{i(1+i)^{20} - 1} = 0.0802$$

With the operation of 350 days per year and NH_3 production rate of 1000 kg day^{-1}, the electrolyzer cost per kg of NH_3 is:

$$Electrolyzer\ cost = 2508290.4\ USD \times \frac{0.0802}{350 days} \times \frac{1}{1000 kg/day} = 0.574\ USD kg{NH_3}^{-1}$$

Capital cost:

$$Capital\ cost\ =\ Electrolyzer\ cost + catalyst\ cost\ + KOH\ cost = 0.632\ USDkgNH_3{}^{-1}$$

Balance of plant cost:

$$Balance\ of\ plant\ cost\ = Electrolyzer\ cost \times 35\% = 0.201\ USDkgNH_3{}^{-1}$$

Maintenance cost:

$$Maintenance\ cost\ = Electrolyzer\ cost \times 2.5\% = 0.014\ USDkgNH_3{}^{-1}$$

Other operational costs:

$$Other\ operational\ cost\ = Electrolyzer\ cost \times 10\% = 0.057\ USDkgNH_3{}^{-1}$$

The power required is calculated by: P = UI ($U = E_{ox}^{0} - E_{re} + E_1, where\ E_{ox}^{0} = 1.23\ V, E_{re}\ is\ the\ cathodic\ potetial, E_1\ is\ the\ overp$)

$$Power\ required = 1.73\ V \times 558449A \times \frac{MW}{10^6 W} = 0.966\ MW$$

Electricity cost:

$$Electricity\ cost = \frac{0.966\ MW}{1000\frac{kW}{MW}} \times 24h \times \frac{0.03USD}{kWh} \times \frac{1}{1000kg/day} = 0.697\ USD\ kgNH_3{}^{-1}$$

Product separation costs:

$$Product\ separation\ costs = Electricity\ cost\ \times 10\% = 0.07\ USD\ kgNH_3{}^{-1}$$

The water flow rate needed for anodic OER reaction is:

$$H_2O\ in\ anode = 558449A \times \frac{1}{4e^- \times \frac{96485C}{mol}} \times \frac{0.018kg}{mol} \times \frac{0.2642\ gal}{kg} \times \frac{86400s}{day} = 594.718\frac{gal}{day}$$

Water Cost:

$$Water\ cost = 594.718\frac{gal}{day} \times \frac{0.0054\ USD}{gal} \times \frac{1}{1000kg/day} = 0.003\ USDkgNH_3{}^{-1}$$

Total cost:

$$\begin{aligned} Total\ cost \\ &= 0.632\ USDkgNH_3{}^{-1} + 0.201\ USDkgNH_3{}^{-1} + 0.014\ USDkgNH_3{}^{-1} \\ &NH_3{}^{-1} + 0.697\ USD\ kgNH_3{}^{-1} + 0.07\ USD\ kgNH_3{}^{-1} + 0.003\ USDkgN \\ &= 1.674\ USDkgNH_3{}^{-1} \end{aligned}$$

When dilute nitrate-contaminated water is considered as the feed, nitrate pre-concentration introduces

an additional cost. Concentrating NO_3^- from 0.5 mM to 0.1 M requires an approximately 200-fold enrichment.[21,22] Based on reported electrodialysis energy consumption and extrapolation to this concentration factor, the additional electricity demand is estimated to be approximately 28 kWh $kgNH_3^{-1}$, corresponding to 0.84 USD $kgNH_3^{-1}$ at an electricity price of 0.03 USD kWh^{-1}. Accordingly, the ammonia production cost would increase from 1.674 to approximately 2.514 USD $kgNH_3^{-1}$.

Table S6 Comparing the performance of our work with other reported electrocatalysts for NO_3RR.

Material	**electrolyte**	**Potential (V)**	**Faradic Efficiency (%)**	**Yield Rate ($mg \cdot h^{-1} \cdot mg^{-1}$)**	**Energy Efficiency (%)**	**Ref.**
A-$CoFe_{0.25}Cr_{1.75}O_4$	1M KOH + 0.1M KNO_3	−0.1	94	17.23	35.4	**This work**
CuCo nanosheets	1M KOH + 0.1M KNO_3	−0.1	60	1.00	22.7	[23]
CoP-CNS	1M KOH + 0.1M KNO_3	−0.1	58	0.80	21.9	[24]
NiFe-LDH	1M KOH + 0.1M KNO_3	−0.1	80	3.08	30.2	[25]
Ni0.75Fe0.25(OH)2	1M KOH + 0.1M KNO_3	−0.1	75	1.28	28.35	[26]
NiNC	0.1 M NaOH + 0.5 M $NaNO_3$	−0.1	55	0.12	21.04	[27]
CuNC	0.1 M NaOH + 0.5 M $NaNO_3$	−0.1	20	0.50	5.98	[27]
Fe-PPy	0.1 M KOH + 0.1 M KNO_3	−0.3	100	1.02	35.12	[28]
CrNC	0.05 M PBS + 0.16 M KNO_3	−0.2	92	0.34	28.94	[29]
MnNC	0.05 M PBS + 0.16 M KNO_3	−0.2	90	0.05	27.68	[29]
FeNC	0.05 M PBS + 0.16 M KNO_3	−0.2	75	0.02	23.25	[29]
CuNC	0.05 M PBS + 0.16 M KNO_3	−0.2	82	0.07	26.25	[29]

MoNC	0.05 M PBS + 0.16 M KNO_3	−0.2	55	0.07	17.24	[29]
PdNC	0.05 M PBS + 0.16 M KNO_3	−0.2	65	0.05	18.50	[29]
LaNC	0.05 M PBS + 0.16 M KNO_3	−0.2	40	0.05	12.18	[29]
CeNC	0.05 M PBS + 0.16 M KNO_3	−0.2	80	0.05	24.36	[29]
Cu_2O NCs	0.1 M $NaSO_4$ + 8 mM $NaNO_3$	−0.3	93	7.58	26.07	[30]
CuCo aerogel	1.0 M KOH + 0.07 M KNO_3	−0.2	98	35.94	36.64	[31]
Ru	H-B process	-	-	1.03	61	[32]

Table S7 The parameters related to Nyquist plots.

Sample	R_s/ Ω	R_{ct}/ Ω	CPE_{dl}
$CoFe_{0.25}Cr_{1.75}O_4$	5.02	61.79	0.955
A-$CoFe_{0.25}Cr_{1.75}O_4$	5.29	10.21	0.441
$Co_{0.8}Fe_{0.2}(OH)_2$	5.60	9.43	0.485

References

1. Kresse, G. & Furthmuller, J. Efficient iterative schemes for Ab initio total-energy calculations using a plane-wave basis set. *Phys. Rev. B: Condens. Matter Mater. Phys.* **54**, 11169 (1996).
2. Blöchl, P. E. Projector augmented-wave method. *Phys. Rev. B: Condens. Matter Mater. Phys.* **50**, 17953 (1994).
3. Kresse, G. & Joubert, D. From ultrasoft pseudopotentials to the projector augmented wave method. *Phys. Rev. B: Condens. Matter Mater. Phys.* **59**, 1758 (1999).
4. Chen, X., Cheng, Y., Zhang, B., Zhou, J. & He, S. Gradient-concentration RuCo electrocatalyst for efficient and stable electroreduction of nitrate into ammonia. *Nat. Commun.* **15**, 6278 (2024).
5. Grimme, S. Semiempirical GGA-type density functional constructed with a long-range dispersion correction. *J. Comput. Chem.* **27**, 1787 (2006).
6. Wang, V., Xu, N., Liu, J., Tang, G. & Geng, W.-T. VASPKIT: a user-friendly interface facilitating high-throughput computing and analysis using VASP code. *Comput. Phys. Commun.* **267**, 108033 (2021).
7. Nørskov, J. K.; Rossmeisl, J.; Logadottir, A.; Lindqvist, L.; Kitchin, J. R.; Bligaard, T.; Jonsson, H. J. K. Origin of the Overpotential for Oxygen Reduction at a Fuel-Cell Cathode. *J. Phys. Chem. B* **108**, 17886−17892 (2004).
8. Peterson, A. A.; Abild-Pedersen, F.; Studt, F.; Rossmeisl, J.; Nørskov, J. K. How copper catalyzes

the electroreduction of carbon dioxide into hydrocarbon fuels. *Energy Environ. Sci.* **3**, 1311−1315 (2010).
9. Wu, Q.; Dai, C.; Meng, F.; Jiao, Y.; Xu, Z. J. Potential and electric double-layer effect in electrocatalytic urea synthesis. *Nat. Commun.* **15**, 1095 (2024).
10. Mathew, K.; Sundararaman, R.; Letchworth-Weaver, K.; Arias, T. A.; Hennig, R. G. Implicit solvation model for density-functional study of nanocrystal surfaces and reaction pathways. *J. Chem. Phys.* **140**, No. 084106 (2014).
11. Taylor, C. D.; Wasileski, S. A.; Filhol, J.-S.; Neurock, M. First principles reaction modeling of the electrochemical interface: Consideration and calculation of a tunable surface potential from atomic and electronic structure. *Phys. Rev. B: Condens. Matter Mater. Phys.* **73**, 165402 (2006).
12. Duan, Z.; Henkelman, G. Surface charge and electrostatic spin crossover effects in CoN4 electrocatalysts. *ACS Catal.* **10**, 12148−12155 (2020).
13. Wang, Y., Yu, Y., Jia, R., Zhang, C. & Zhang, B. Electrochemical synthesis of nitric acid from air and ammonia through waste utilization. *Natl. Sci. Rev.* **6**, 730–738 (2019).
14. Dai, C. et al. Suppressing product crossover and CC bond cleavage in a glycerol membrane electrode assembly reformer. *Energy Environ. Sci.* **17**, 6350–6359 (2024).
15. Bertuccioli, L. et al. Study on development of water electrolysis in the EU. (2014). https://www.fch.europa.eu/sites/default/files/FCHJUElectrolysisStudy_FullReport%20(ID%2019 9214).pdf.
16. James, B., Colella, W., Moton, J. PEM Electrolysis H2A Production Case Study Documentation. (2013). https://www.nrel.gov/hydrogen/assets/pdfs/h2a-pem-electrolysis-case-study-documentation.pdf.
17. International Renewable Energy Agency. Renewable power generation costs in 2022. (2023). https://www.irena.org/Publications/2023/Aug/Renewable-Power-GenerationCosts-in-2022.
18. Jouny, M., Luc, W., Jiao, F. General Techno-Economic Analysis of CO_2 Electrolysis Systems. *Ind. Eng. Chem. Res.* **57**, 2165-2177 (2018).
19. Fan, K. et al. Active hydrogen boosts electrochemical nitrate reduction to ammonia. *Nat. Commun.* **13**, 7958 (2022).
20. Chen, F. Y. et al. Electrochemical nitrate reduction to ammonia with cation shuttling in a solid electrolyte reactor. *Nat. Catal.* **7**, 1032–1043 (2024).
21. Niemann, V. A., et al. Co-designing electrocatalytic systems with separations to improve the sustainability of reactive nitrogen management. *ACS Catal.* **13**, 6268-6279 (2023).
22. Mohammadi, R., Ramasamy, D. L., Sillanpää, M. Enhancement of nitrate removal and recovery from municipal wastewater through single-and multi-batch electrodialysis: Process optimisation and energy consumption. Desalination, **498**, 114726 (2021).
23. J. Fang, Q. Zheng, Y. Lou, K. Zhao, S. Hu, G. Li, O. Akdim, X. Huang and S. Sun, *Nat. Commun.*, 2022, **13**, 7899.
24. K. Fan, W. Xie, J. Li, Y. Sun, P. Xu, Y. Tang, Z. Li and M. Shao, *Nat. Commun.*, 2022, **13**, 7958.
25. F. Dionigi and P. Strasser, *Adv. Energy Mater.*, 2016, **6**, 1600621.
26. L. Trotochaud, S. L. Young, J. K. Ranney and S. W. Boettcher, *J. Am. Chem. Soc.*, 2014, **136**, 6744–6753.
27. D. S. Braga, et al. In Situ Structural Evolution and Activity Descriptor of Atomically Dispersed Catalysts During Nitrate Electroreduction. *Adv. Sci.* **12**, e10282 (2025).
28. P. Li, Z. Jin, Z. Fang, G. Yu, A single-site iron catalyst with preoccupied active centers that achieves selective ammonia electrosynthesis from nitrate *Energy Environ. Sci.* 2021, **14**, 3522–3531.
29. E. Murphy, et al. Elucidating electrochemical nitrate and nitrite reduction over atomically-dispersed transition metal sites *Nat. Commun.* 2023, **14**, 4554.

30. L. Bai, et al. Electrocatalytic Nitrate and Nitrite Reduction toward Ammonia Using Cu_2O Nanocubes: Active Species and Reaction Mechanisms *J. Am. Chem. Soc.* 2024, **146**, 9665–9678.
31. Z. Jiang, et al. High-Performance CuCo Aerogel Electrocatalyst for Relay Electroreduction of Nitrate to Ammonia *Adv Funct Materials* 2025, **35**, 2507903.
32. M. Kitano, et al. Self-organized Ruthenium–Barium Core–Shell Nanoparticles on a Mesoporous Calcium Amide Matrix for Efficient Low-Temperature Ammonia Synthesis *Angew. Chem. Int. Ed.* 2018, **57**, 2648–2652.